

# Relaxation Phenomena in Nonlinear Optical Polymers

T. Weyrauch and W. Haase

## 12.1 Introduction

Polymeric non-linear optical (NLO) materials have attracted much attention during the last two decades because of their potential to surpass the performance of current inorganic materials such as  $\text{LiNbO}_3$  in integrated high-speed electro-optic devices. Since the optical nonlinearity in polymers is based on molecular properties of chromophores, molecular design allows to tailor the material properties and thus to achieve high electro-optic coefficients. Other important advantages of polymers are the low dispersion between carrier and modulation frequency (allowing high-speed operation), their compatibility with many substrates, a flexibility of fabrication methods, and therefore the prospect of large-scale low-cost integration (see e.g. [1, 2]).

The polar symmetry that is required for second-order (quadratic) non-linear optical properties has been a main point of interest since the first description of such properties in polymers [3], because the non-centrosymmetry has to be induced for amorphous polymers by a poling process: The polymers are cooled down from temperatures above to well below the glass transition point while a high d.c. electric field is applied and a frozen-in polar order of dipolar chromophores remains even after the d.c. poling field is switched off. However, the glassy state allows for structural relaxations and a decay of quadratic NLO properties can be observed. Investigations on the poling and its relaxation processes have thus been major topics in research and development of NLO polymer materials and devices. The activity in this field led also to the development of new experimental techniques that are now used far beyond their original scope.

In this paper we will briefly review the basic principles of NLO polymers. Then experimental techniques and results performed to study the relaxation of polar order will be presented. We will show that the observed relaxation behavior can be described in terms of a relaxation model for structural relaxations in the glassy state. Finally the application of electroabsorption spectroscopy for evaluation of relaxation processes will be discussed.

## 12.2 Physical background

### 12.2.1 NLO susceptibility and effects

In nonlinear optical media the linear relationship between an electric field  $\mathbf{E}$  and the induced polarization  $\mathbf{P}$  must be replaced by a nonlinear expression, e.g. a Taylor series expansion:

$$P_i = P_i^{(0)} + \sum_j \chi_{ij}^{(1)} E_j + \sum_{jk} \chi_{ijk}^{(2)} E_j E_k + \sum_{jkl} \chi_{ijkl}^{(3)} E_j E_k E_l + \dots \quad (12.1)$$

Here the indices  $i, j, k, l$  denote the vector components in the laboratory frame,  $\mathbf{P}^{(0)}$  is a permanent polarization that may be present in the material,  $\chi^{(1)}$  is the linear optical susceptibility and  $\chi^{(2)}, \chi^{(3)}, \dots$  are the nonlinear susceptibilities of second, third,  $\dots$  order, respectively. For quadratic effects we have to take into account only the term containing  $\chi^{(2)}$  and we obtain for the related quadratic polarization

$$P_i^{(2)} = \sum_{jk} \chi_{ijk}^{(2)} E_j E_k. \quad (12.2)$$

Quadratic effects require a non-centrosymmetric material structure. Otherwise, an inversion operator applied to (12.2) would invert the sign of the electric polarization vector component  $P_i^{(2)}$  and the electric field vector components  $E_j$  and  $E_k$ , but not of the  $\chi^{(2)}$  tensor, a contradiction that can only be solved if all components of  $\chi^{(2)}$  are zero. For non-centrosymmetric materials however the inversion operator will also change the sign of the  $\chi^{(2)}$  components.

Equation (12.2) describes the interaction of three waves. This can be seen best considering the total electric field applied to the material consisting of two Fourier components  $E(\omega_1)$  and  $E(\omega_2)$ :

$$P_i^{(2)}(\omega_3) = \sum_{jk} \chi_{ijk}^{(2)}(\omega_3; \omega_1, \omega_2) E_j(\omega_1) E_k(\omega_2) + \dots \quad (12.3)$$

Thus, the nonlinear  $\chi^{(2)}$  term is the origin of the generation of the sum and the difference frequencies  $\omega_3 = \omega_1 + \omega_2$ ,  $\omega'_3 = \omega_1 - \omega_2$ . Two special cases deserve special attention: First, in the case  $\omega_1 = \omega_2$  we have frequency doubling (second harmonic generation, SHG), which may occur as the self-interaction of a single optical wave. Second, if one electric field is an optical wave and the other is a static (or quasi-static low frequency) field the interaction appears as a (static or low-frequency) refractive index variation for the light beam. This is known as Pockels effect and the basis for interferometric electrooptic modulators.

### 12.2.2 Organic NLO materials

In organic materials the origin of the optical nonlinearity is the nonlinear behavior on the molecular level. The dipole moment of a molecule under a local electric field  $\mathbf{E}^{\text{loc}}$  may be described similar to (12.1) as a Taylor expansion:

$$\mu_I = \mu_I^0 + \sum_J \alpha_{IJ} E_J + \sum_{JK} \beta_{IJK} E_J E_K + \sum_{JKL} \gamma_{JKL} E_J E_K E_L + \dots \quad (12.4)$$

Here  $\mu^0$  is the permanent dipole moment,  $\alpha$  is the linear polarizability and  $\beta$ ,  $\gamma$  are the quadratic and cubic hyperpolarizabilities, respectively. A well known type of molecules, representing materials with high quadratic hyperpolarizability, are extended  $\pi$ -electron systems with donor and acceptor substituting groups (Fig. 12.1). The  $\pi$ -electron system may be realized e.g. by phenyl, stilbene or azobenzene groups. The nitro and the dialkylamino groups are often used as donor and acceptor groups, respectively. The  $\beta$  tensor of such rod-like NLO molecules has one dominant component  $\beta_{ZZZ}$ , where  $Z$  is the molecular longitudinal axis. Other components are much smaller and can usually be neglected.

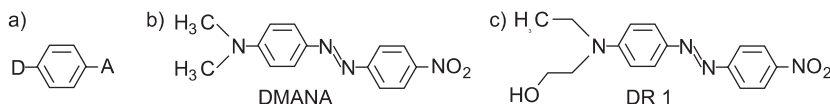


**Fig. 12.1.** Quadratic NLO chromophores. (a) General structure (D = donor group, A = acceptor group). (b),(c) Example molecules

In organic materials intramolecular forces are much higher than intermolecular forces and the macroscopic susceptibility may easily be calculated from the hyperpolarizabilities of the molecules in the ensemble by considering their orientational average [4–6]:

$$\chi_{ijk}^{(2)}(-\omega_3; \omega_1, \omega_2) = (N/V) f_i^{\omega_3} f_j^{\omega_1} f_k^{\omega_2} \langle \beta_{IJK} \cos \xi_{iI} \cos \xi_{jJ} \cos \xi_{kK} \rangle \quad (12.5)$$

$N/V$  is the number of molecules per volume unit,  $\xi_{iI} = \angle(i, I)$ ,  $\xi_{jJ} = \angle(j, J)$  and  $\xi_{kK} = \angle(k, K)$  describe the relative orientation of the molecular frame  $(I, J, K)$  and the laboratory frame  $(i, j, k)$ . The angle brackets  $\langle \dots \rangle$  denote averaging over all molecules in the ensemble. The local field correction factors  $f_i^{\omega}$  describe the relation between the externally applied field  $\mathbf{E}$  and the local field  $\mathbf{E}^{\text{loc}}$  sensed by the molecules.

### 12.2.3 Poled NLO polymers

A poling procedure is necessary to introduce a non-centrosymmetric structure in amorphous polymers. For thermal poling (as shown in Fig. 12.2a) the

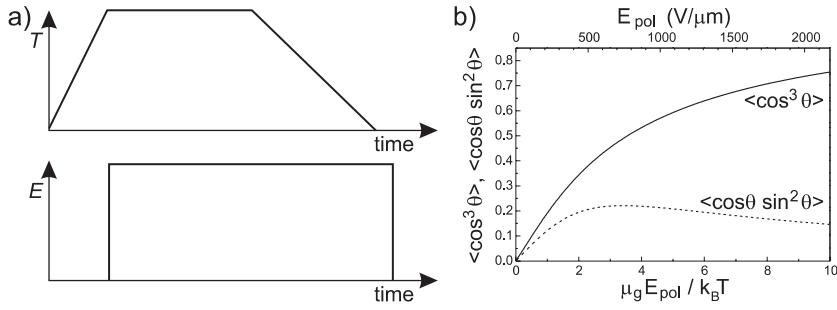


**Fig. 12.2.** Thermal poling. (a) Schematic of the evolution of temperature  $T$  and electric poling field  $E$ . (b) Expectation values for the polar order parameters  $\langle \cos^3 \theta \rangle$  and  $\langle \cos \theta \sin^2 \theta \rangle$

polymer is heated to or above the glass transition point and a high electric field is applied. Subsequently the polymer is cooled down to room temperature under the field. At low temperatures the induced polar structure is frozen in and the external electric field can be switched off. The resulting structure of the polymer has an  $\infty mm$  symmetry and the  $\chi^{(2)}$  tensor has only two independent elements  $\chi_{zzz}^{(2)}$  and  $\chi_{zxx}^{(2)}$  (if additional symmetry considerations are valid [7]). Thus (12.5) results in

$$\chi_{zzz}^{(2)}(-\omega_3; \omega_1, \omega_2) = (N/V) f_z^{\omega_3} f_z^{\omega_1} f_z^{\omega_2} \beta_{ZZZ} \langle \cos^3 \theta \rangle \quad (12.6)$$

$$\chi_{zxx}^{(2)}(-\omega_3; \omega_1, \omega_2) = 0.5(N/V) f_z^{\omega_3} f_x^{\omega_1} f_x^{\omega_2} \beta_{ZZZ} \langle \cos \theta \sin^2 \theta \rangle, \quad (12.7)$$

where the terms  $\langle \cos^3 \theta \rangle$  and  $\langle \cos \theta \sin^2 \theta \rangle$  are the relevant polar order parameters. Their expectation values can be calculated from the Maxwell–Boltzmann distribution of the dipoles in the poling field [5, 8]. Figure 12.2b shows the order parameters in dependence on the Boltzmann factor  $\mu_g E_{\text{pol}}^{\text{loc}} / k_B T$  ( $\mu_g$  = permanent dipole moment,  $E_{\text{pol}}^{\text{loc}}$  = local electric poling field,  $k_B$  = Boltzmann constant,  $T$  = temperature). The scale for the electric field refers to an example of  $\mu_g = 7$  Debye and  $T = 100^\circ\text{C}$ . Note that a local field correction factor  $f^0 = f^{\omega=0}$  describes the relation between external and local poling field. The Onsager and the Lorentz–Lorenz models have been widely used for the calculation of  $f^0$  and  $f^\omega$ , the d.c. and optical local electric field correction, respectively [5, 9], but alternative models, that consider the anisotropic shape of molecules, e.g. [10], deliver non-negligible different results. The uncertainty in the determination of the correction factors is in general a problem for the exact calculation of the relationship between molecular and macroscopic NLO properties.

#### 12.2.4 Stark effect (Electroabsorption)

In quadratic NLO materials the absorption is influenced by an electric field simultaneously to the refractive index (electroabsorption and electrooptic effect,

or Stark effect and Pockels effect, respectively) and both effects are connected due to the Kramers–Kronig relation. Thus the Stark effect may be discussed in terms of the imaginary parts of the nonlinear optical tensors  $\chi^{(2)}$ ,  $\beta$ ,  $\chi^{(3)}$  and  $\gamma$  for the linear and the quadratic effect, respectively [11]. We use here a description, where the Stark effect is immediately related to relevant molecular properties of the chromophores, i.e. the differences of dipole moment ( $\Delta\mu$ ) and linear polarizability ( $\Delta\alpha$ ) in the ground and the electronically excited state [12]. The shift  $\Delta\tilde{\nu}$  of the wave number of the absorption band of an orientationally fixed molecule by application of an electric field  $\mathbf{E}$  is given by

$$(h/c)\Delta\tilde{\nu} = \Delta\mu \mathbf{E}^{\text{loc}} - (1/2)\Delta\alpha \mathbf{E}^{\text{loc}} \mathbf{E}^{\text{loc}} \quad (12.8)$$

( $c$  = light velocity,  $h$  = Planck constant). Note, that (12.8) contains the local electric field  $\mathbf{E}^{\text{loc}} = f\mathbf{E}$ ; again a local field correction factor  $f$  is required to obtain it from the external field  $\mathbf{E}$ .  $\Delta\tilde{\nu}$  is usually too small (especially in comparison to the width of the absorption band) to be measured directly. We rather consider the change of the extinction  $\Delta\varepsilon(\tilde{\nu})$  at fixed  $\tilde{\nu}$  and derive from (12.8) for a single molecule [12]

$$\Delta\varepsilon(\tilde{\nu}) = \frac{\Delta\mu}{hc} \mathbf{E}\tilde{\nu} \frac{d(\varepsilon/\tilde{\nu})}{d\tilde{\nu}} + \frac{(\Delta\mu \mathbf{E})^2}{2(hc)^2} \tilde{\nu} \frac{d^2(\varepsilon/\tilde{\nu})}{d\tilde{\nu}^2} + \frac{(\Delta\alpha \mathbf{E})\mathbf{E}}{2hc} \tilde{\nu} \frac{d(\varepsilon/\tilde{\nu})}{d\tilde{\nu}}. \quad (12.9)$$

We can calculate the electric induced absorption change  $\Delta A(\tilde{\nu})$  of a macroscopic sample by averaging (12.9) over all molecules in the ensemble considering of the molecules' orientational distribution in respect to the electric field and the light propagation direction:

$$\begin{aligned} \Delta A(\tilde{\nu}) = & F_1 \frac{\Delta\mu}{hc} \mathbf{E} \mathcal{A}'(\tilde{\nu}) + \frac{1}{2} \frac{E^2}{hc} [\Delta\alpha_l(1 - F_2) + \Delta\alpha_t F_2] \mathcal{A}'(\tilde{\nu}) \\ & + \frac{1}{2} \left( \frac{\Delta\mu}{hc} \mathbf{E} \right)^2 F_2 \mathcal{A}''(\tilde{\nu}), \end{aligned} \quad (12.10)$$

where  $\mathcal{A}'(\tilde{\nu})$  and  $\mathcal{A}''(\tilde{\nu})$  are abbreviations for the derivative terms

$$\mathcal{A}'(\tilde{\nu}) = \tilde{\nu} \frac{d(A/\tilde{\nu})}{d\tilde{\nu}} \quad \text{and} \quad \mathcal{A}''(\tilde{\nu}) = \tilde{\nu} \frac{d^2(A/\tilde{\nu})}{d\tilde{\nu}^2} \quad (12.11)$$

of the absorption spectrum  $A(\tilde{\nu})$  of the sample.  $\Delta\alpha_l$  is the longitudinal component of the polarizability difference,  $\Delta\alpha_t$  is the transversal component and  $F_1$  and  $F_2$  are order parameters given by

$$F_1 = \frac{\langle \cos\theta \sin^2\theta \rangle}{\langle \sin^2\theta \rangle} \quad \text{and} \quad F_2 = \frac{\langle \cos^2\theta \sin^2\theta \rangle}{\langle \sin^2\theta \rangle}. \quad (12.12)$$

$\theta$  is the angle between the dipole moment and the propagation direction of the light. The angle brackets  $\langle \dots \rangle$  denote averaging over all molecules in the sample.  $F_1$  is a polar order parameter, consequently the linear Stark effect

described by the first term of (12.10) can be observed only in polar samples. Since  $F_2$  is a non-polar order parameter the quadratic effect [second and third term in (12.10)] occurs also in unpoled samples. The expectation value of  $F_2$  can be calculated easily to  $1/5$  for isotropic materials, but differs even for poled samples only insignificantly from this value. We can therefore simplify (12.10) by neglecting this small difference as well as the then meaningless polarizability anisotropy by replacing  $F_2$  with  $1/5$  and using  $\Delta\alpha = \Delta\alpha_l = \Delta\alpha_t$ .

### 12.2.5 Piezoelectric effect

Quadratic NLO polymers have a macroscopic polarization due to a frozen-in polar orientation of dipolar chromophores. They can thus be considered as molecular dipole electrets with additional polarization-related properties as e.g. piezo- and pyroelectricity. We paid some attention to the characterization of poling stability by the piezoelectric effect because rather simple experimental techniques (acoustoelectric measurements) may be used. Broadhurst et al. provided a theoretical description of the piezoelectricity in molecular dipole electrets [13, 14]. We present their results here briefly: The frozen-in polarization  $P$  of a molecular dipole electret is given by

$$P = \frac{N}{V} \langle m \rangle, \quad (12.13)$$

where  $N/V$  is the number of dipoles per volume and  $\langle m \rangle$  is the effective molecular dipole moment, which is composed from the permanent dipole moment  $\mu_g$  and an internal-field-induced contribution. Calculation of  $\langle m \rangle$  results in

$$P = \frac{N}{V} \frac{\epsilon_\infty + 2}{3} \mu_g \langle \cos \theta \rangle, \quad (12.14)$$

with the dielectric constant  $\epsilon_\infty$  at optical frequencies and the average  $\langle \cos \theta \rangle$  of the angle between individual molecular dipoles and the polar axis of the material. Rather than the variation of the polarization  $P$  that is induced by a change of the pressure  $p$ , one measures experimentally the change of the compensation charges  $Q$  on the electrode area  $A$  of the sample, i.e.

$$d_p^{\text{exp}} = \frac{1}{A} \frac{\partial Q}{\partial p}, \quad (12.15)$$

which can be approximately described by

$$d_p^{\text{exp}} = -P\beta \frac{\epsilon_\infty}{3} = -\beta \frac{N}{V} \frac{(\epsilon_\infty + 2)\epsilon_\infty}{9} \mu_g \langle \cos \theta \rangle, \quad (12.16)$$

where  $\beta = -(dV/dp)/V$  is the volume compressibility. The piezoelectric coefficient is proportional to the induced polarization, i.e. to the average value  $\langle \cos \theta \rangle$ . This is a different dependency on molecular order than in the case of the nonlinear optical susceptibilities, where higher order terms are used (12.6). Thus one can't necessarily expect a similar relaxation behavior of NLO and piezoelectric properties.

## 12.3 The stability of polar order after poling

### 12.3.1 Experimental methods

#### Sample preparation and poling

Investigations on NLO polymers require very often thin film samples, prepared using the spin coating technique, where the polymer is dissolved in an appropriate solvent and the solution is spread onto a substrate, e.g. glass, mounted on top of a rotating table. The film thickness can be set from the sub-micrometer range until several micrometers by varying the polymer concentration and the rotation speed. For drying one usually keeps the films after their preparation for several hours under room ambient conditions and subsequently heats them under vacuum to remove the remaining solvent.

In most cases poling field is applied perpendicular to the film plane and the substrate must comprehend a conductive layer used as an electrode. If a transparent substrate is required, the electrode usually consists of indium tin oxide (ITO). Two different poling techniques, electrode poling and corona poling, have been used. For the first an additional electrode layer must be provided, e.g. by sputtering a thin metal layer onto the polymer film or attaching a second ITO covered substrate onto the polymer film using an epoxy resin [12]. The demand for a sophisticated sample preparation is one central problem of electrode poling. Any defect in the film (originated from dust or impurities in polymer or solvent) may lead to an electric short circuit when a high poling voltage at an elevated temperature is applied and thus destroy the sample. The absorption of metal electrodes, although semi-transparent for sufficiently thin layers, raise another problem for experiments where higher light intensities are necessary as e.g. in SHG measurements.

Corona poling does not require a second electrode, but uses the corona discharge at a needle tip or a thin wire connected to a high voltage  $U_{HV}$  (about 10 kV) to generate ions above a polymer sample (see Fig. 12.3). Grounding the ITO electrode of the sample forces the ions to follow the electric field onto the polymer film's surface, where they remain for some time until they are

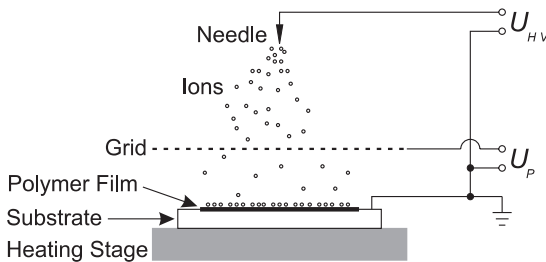


**Fig. 12.3.** Schematics of a corona poling setup ( $U_{HV}$  high voltage,  $U_P$  poling voltage)

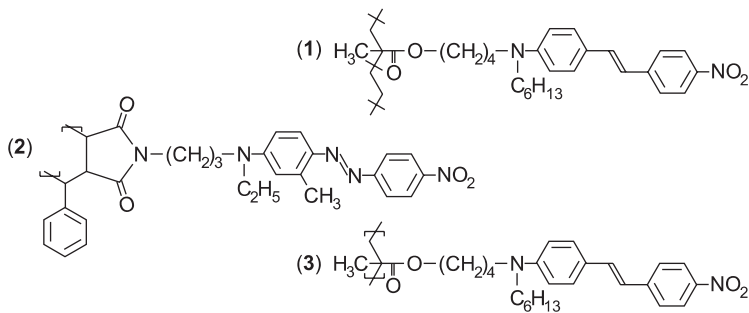


**Fig. 12.4.** Chemical structure of polymers used for poling and relaxation experiments

neutralized. Hence a rather high voltage is applied across the polymer film. In a more sophisticated version of the technique an additional grid is used between the corona and the film that allows to control the poling voltage, which will not exceed the intermediate voltage  $U_P$  applied to the grid. The major advantage of corona poling is the much less demanding sample preparation: Local defects do not destroy the whole sample because of the low lateral conductivity for the ions on the polymer surface and the remaining part of the film can be poled without damage. A disadvantage of corona poling is a possible impairment of the surface quality through the ion bombardment. The ions may also induce chemical reactions with the polymer or the NLO chromophores and thus deteriorate the sample. Controlling the corona poling atmosphere, esp. using an oxygen-free gas, can reduce the negative effects [15].

We present here results that were obtained from measurements on the polymers depicted in Fig. 12.4. Polymer **1** is a copolymer of ethylene and methacrylate units, the latter are attached by an  $\text{O}(\text{CH}_2)_4$  spacer to an amino nitrostilbene NLO chromophore. The ratio of ethylene and methacrylate is 9:1; the glass transition temperature is about  $103^\circ\text{C}$ . The poly(styrene-maleic anhydride) polymer **2** with a chemically attached Disperse Red 1 side group was provided by Sandoz Optoelectronics (Huningue, France). The glass transition is at  $137^\circ\text{C}$ . The polymethacrylate **3** has an amino nitrostilbene NLO side group and a glass transition temperature of about  $66^\circ\text{C}$ . Polymers **1** and **3** were provided by Merck KGaA (Darmstadt, Germany).

## Second harmonic generation

We used the Maker-fringe technique [16] to determine the stability of the optical nonlinearity in poled polymers. The pulsed laser beam of a Nd-YAG laser ( $\lambda = 1064\text{ nm}$ ) was directed to the sample (the polymer film on a glass substrate), which was mounted on a rotation stage to allow a variation of the angle of incidence  $\alpha$  (Fig. 12.5a). After blocking the fundamental wave the signal strength of the second harmonic light ( $\lambda = 532\text{ nm}$ ) was measured



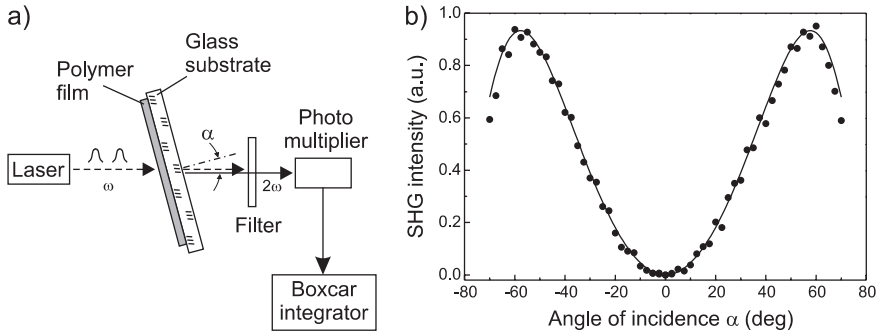


**Fig. 12.5.** (a) Schematics of a SHG experiment using the Maker-fringe technique. (b) Experimental curves of SH intensity vs. angle of incidence  $\alpha$

using a photomultiplier and a Boxcar integrator that measured the signal only during the 10 ns pulses to increase the signal-to-noise ratio. To avoid errors due to fluctuations of the energy of the pulses of the fundamental wave, the polymer second harmonic signal was measured in respect to a reference signal obtained from a quartz crystal. A sample curve of second harmonic intensity versus angle of incidence is shown in Fig. 12.5b. We omit here a discussion of the shape of the curve  $I_{2\omega}(\alpha)$ , which depends not only on the nonlinear susceptibility tensor elements  $\chi_{zzz}^{(2)}$  and  $\chi_{zxx}^{(2)}$ , but also on the refractive indices for the fundamental and second harmonic in polymer and substrate as well as on the sample thickness [5, 8]. For relaxation measurements only the relative signal strength at different times after the poling is relevant and we were able to use the experimental signals directly rather than calculating the nonlinear susceptibility  $\chi^{(2)}$ . Keeping the angle of incidence  $\alpha$  constant allowed for mounting of a corona-poling setup onto the optical table and thus for in situ measurements of the second harmonic intensity during the poling.

### Acoustoelectric measurements

To compare the relaxation of NLO properties and piezoelectricity, we developed acoustoelectric methods for the measurement of the relaxation behaviour of the piezoelectric effect [15, 17]. Both are based on the fact that acoustic waves with relatively moderate pressure suffice to generate an electric response that can be measured by lock-in technique. As shown in Fig. 12.6 the differential pressure of the acoustic sound wave may be applied either transversal (a) or longitudinal (b) to the polar axis of the polymer. Samples for the transversal configuration are prepared by pressing a melted drop of the polymer between two ITO coated glass plates until it reaches the thickness of the spacers that defines the desired distance between the glass plates (typically about 100  $\mu\text{m}$ ). The advantage is the very small amount of polymer that is required for sample preparation, which requires however some experience to avoid parasitic signals (e.g.

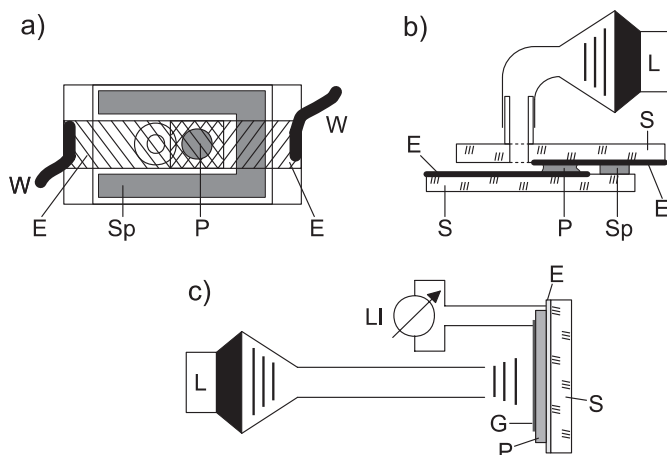


**Fig. 12.6.** Acoustoelectric measurements on poled NLO polymers in (a),(b) transversal and (c) longitudinal geometry (E = electrode, G = gold electrode, L = loudspeaker, LI = lock-in amplifier, P = polymer, S = substrate, Sp = spacer, W = wires)

from the spacers). The disadvantage is the relatively small part of the sample along the edge of the polymer that is deformed by the acoustic pressure and thus contributes to the signal. As shown in [17] the active area corresponds to an annular plate with a width in the order of  $2/3$  of the sample thickness.

Measurements in the longitudinal configuration were performed on spin-casted films with a sputtered top gold electrode. During the poling process the samples were cooled down to the temperature of measurement with a rate of 3 K/min under electric field (corona poling was used for the SHG experiment). For the piezoelectric measurements the electrodes were short-circuited for a few seconds to allow for the discharge of the sample capacitance. The sound signal was generated using the internal signal generator of the lock-in amplifier, an amplifier and a loudspeaker. A funnel and a pipe were used to guide the acoustic wave to the sample.

### 12.3.2 The relaxation of SHG and acoustoelectric response

In in-situ corona poling and SHG experiments we observed two different processes that contribute to the relaxation of second order NLO properties after poling. Figure 12.7a shows the second harmonic power  $P(2\omega)$  during and shortly after corona poling of polymer **1** (Fig. 12.4) at different temperatures. A steep decrease of the SHG signal takes place immediately after switching off the high voltage (at  $t - t_0 = 0$ ), followed by a slower relaxation. The time scale of the faster process is in the order of 1 minute and is generally attributed to the decay of surface charges on the polymer sample. The presence of surface

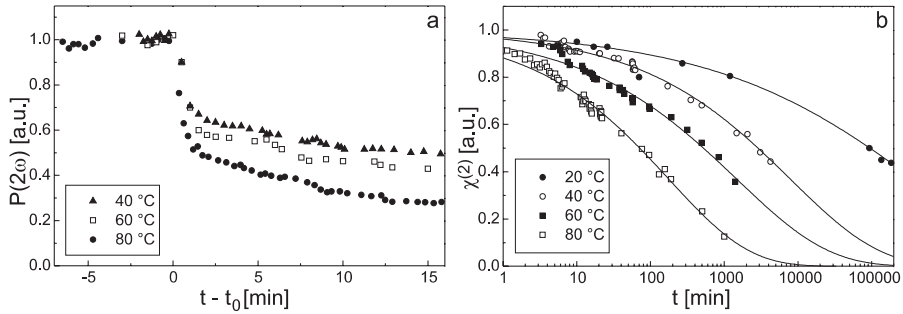


**Fig. 12.7.** (a) SHG signal  $P(2\omega)$  during and immediately after corona poling of the nitrostilbene side-chain polymer **1**. (b) Nonlinear susceptibility  $\chi^{(2)}$  measured in long time experiments at different temperatures

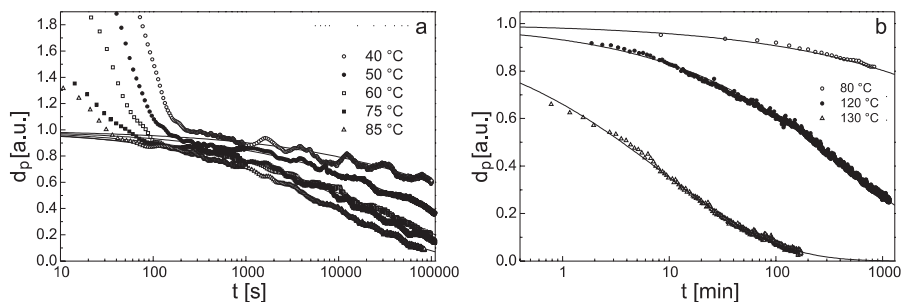
charges, and thus of a poling field, increases the SHG signal by stabilization of the chromophores' polar order in the external d.c. field as well as through higher order nonlinear terms, i.e. from  $\chi^{(3)}(E_{2\omega}; E_{\omega}, E_{\omega}, E_0)$  tensor elements that correspond to the interaction of the d.c. field  $E_0$  and the optical field  $E_{\omega}$ .

Figure 12.7b shows the long term behavior of the nonlinear susceptibility  $\chi^{(2)}$  of polymer **1** at different temperatures. To describe the measured data analytically we tested several different relaxation functions (exponential, bi-exponential, and exponential functions with a time dependent constant as proposed in [18]), but we received the best results using the stretched exponential function

$$u(t) = u_0 \exp[-(t/\tau_0)^\beta], \quad (12.17)$$

also known as the Kohlrausch–Williams–Watt (KWW) function, where the exponent  $\beta$  ( $0 < \beta \leq 1$ ) describes an asymmetrical broadening of the relaxation time distribution. The average relaxation time  $\tau_m = \langle \tau \rangle$  is different from the nominal value  $\tau_0$  and is given by  $\tau_m = (\tau_0/\beta)\Gamma(\beta^{-1})$ , where  $\Gamma$  is the Euler gamma function [19]. The lines in Fig. 12.7b were obtained by fitting KWW functions to the experimental data.

We found a very similar relaxation behavior in acoustoelectric measurements of the piezoelectric effect (Fig. 12.8). Since electrode poling was used for these experiments, the faster process cannot be explained by the presence of ions on the surface, but by charge distributions that are generated due to charge injection at the polymer electrode interfaces. The influence of such charges on the acoustoelectric signal is however different from NLO experiments, because rather high piezoelectric signals may arise from asymmetric volume charge distributions directly, i.e. even without a polar order of the NLO chromophores. Indeed, we observed rather high acoustoelectric signal amplitudes during the fast process immediately after the poling ended, esp. in case of the transversal experiment (cf. Fig. 12.8a, where the sample is deformed non-homogeneously). The decay times of these fast processes are comparable



**Fig. 12.8.** Relaxation of the piezoelectric signal  $d_p$  in acoustoelectric experiments (a) measured in transversal geometry on a sample of polymer **1**, (b) obtained from longitudinal experiments on polymer **2**

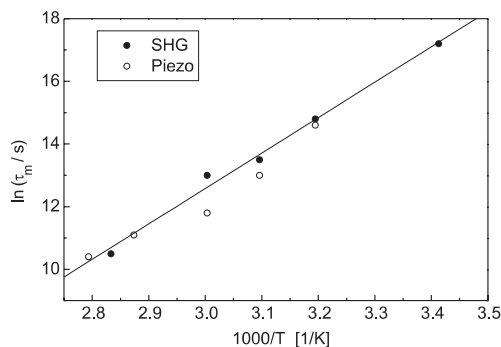


**Fig. 12.9.** Temperature dependence of the average relaxation time  $\tau_m$  of the polymer **1** obtained from relaxation data of SHG and piezoelectric (acoustoelectric) effect

to those observed in transient depolarization current measurements [15, 20], which is another indication for their relation to charge distributions.

Fitting the KWW function to experimental curves of both, the piezoelectric effect and SHG measured on samples of the polymer **1** we found values for  $\beta$  in the range from 0.35 to 0.45 for the temperature between 40 °C and 85 °C. An example for the temperature dependence of the average relaxation time  $\tau_m$  is shown in Fig. 12.9. The experimental values of  $\tau_m$  follow in a good approximation an Arrhenius-type temperature behavior [15, 21].

### 12.3.3 Discussion of poling stability

An interpretation of the experimental results is possible in terms of semi-empirical phenomenological models, which describe the glass transition as a relaxational phenomenon: Below the transition temperature the characteristic time constant of the structural relaxations of the polymer chains exceeds the time scale set by the experiment, thus the polymer appears as rigid. Above

the glass transition temperature a deviation from Arrhenius behavior is observed for the  $\alpha$  relaxation, i.e. the large scale microbrownian motion of the chains, with a strong slowing down of the relaxation when approaching the glass transition temperature. This temperature dependence of the relaxation time  $\tau$  is often described by the equation given by Williams, Landel and Ferry

$$\ln \left[ \frac{\tau_m(T)}{\tau(T_g)} \right] = \frac{-C_1(T - T_g)}{C_2 + (T - T_g)}, \quad (12.18)$$

known as WLF behavior, where  $\tau(T_g)$  is the relaxation time constant at the glass transition temperature  $T_g$ , and  $C_1$  and  $C_2$  are material constants, which are very often close to the “standard” values  $C_1 = 17$  and  $C_2 = 52$  K [22]. Equation (12.18) implies an infinitely large relaxation time for the temperature  $T_g - C_2$ . Therefore its validity is typically limited to the temperature range above  $T_g + 10$  K. A theoretical foundation for the WLF behavior (Adams–Gibbs–DiMarzio theory) was presented in [23, 24] and based on calculations of the configuration entropy.  $T_0 = T_g - C_2$  was identified as the temperature where the configuration entropy becomes zero.

In the glassy state the relaxation time  $\tau$  depends, in general, not only on  $T$  but also on the material history, hence the material is not in an thermal equilibrium. Non-equilibrium behavior is often described by means of the fictive temperature  $T_f$  introduced by Tool [25]. It corresponds to the temperature of an equilibrium state, which is fictive and could be reached only by infinitely slow cooling, and is equivalent to the actual non-equilibrium state of the material. Figure 12.10 illustrates the fictive temperature concepts by means of the generalized temperature dependence of a thermodynamical quantity  $\phi$ . The measurable temperature dependence  $\phi(T)$  has distinctively different slopes above and below the glass transition temperature (a) and (c), respectively, with a transition region (b) around  $T_g$ . The exact shape of (b) and (c) depends on the history of the material (cooling rate, aging, etc.).

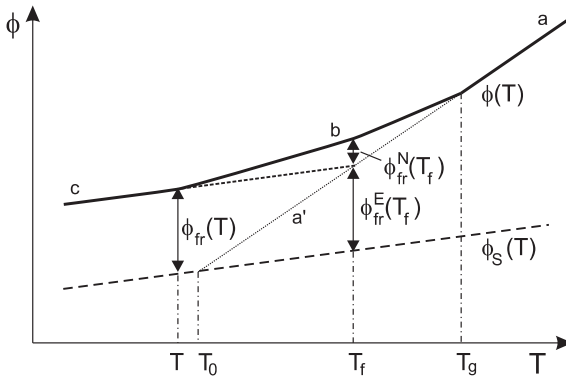


**Fig. 12.10.** Schematic of the temperature dependence of a thermodynamical quantity  $\phi$  for a glass forming material

Curves (a) and (a') describe the material in an equilibrium state, the extrapolation (a') is however a fictive curve for infinitively slow cooling, which is required to allow for slow structural relaxations. This extrapolation ends at the intersection with curve  $\phi_S(T)$ , which is valid for a fictive equilibrium solid state. The free part  $\phi_{fr}$ , i.e. the portion of  $\phi$  that can be attributed to structural relaxation, is given by the difference between  $\phi(T)$  and  $\phi_S(T)$ , and can be divided into an equilibrium part  $\phi_{fr}^E$  below (a') and a non-equilibrium part  $\phi_{fr}^N$  above (a'). The fictive temperature  $T_f$  for a given state  $\phi(T)$  is defined by  $\phi_{fr}^E(T) = \phi_{fr}(T)$ .

If we identify the quantity  $\phi$  with the enthalpy  $H$ , then the slopes of the curve parts (a) and (b) are the heat capacities  $c_p^l$  and  $c_p^g$  for the liquid and glassy state, respectively, and may be obtained by extrapolation of an experimental  $c_p(T)$  curve. The fictive temperature may thus be calculated from experimental data by numerical integration of the equation

$$\frac{dT_f(T)}{dT} = \frac{c_p(T) - c_p^g(T)}{c_p^l(T) - c_p^g(T)}. \quad (12.19)$$

We used differential scanning calorimetry (DSC) to measure  $c_p(T)$ . In Fig. 12.11a two different experimental curves are shown, obtained after annealing the polymer **1** at 80 °C for 20 and 75 minutes. Using (12.19) we obtained the curves for the fictive temperatures  $T_f(T)$  shown in Fig. 12.11b. They demonstrate that the fictive temperature is mainly determined by the material-history-dependent magnitude of the DSC nose at the glass transition and is nearly independent from  $T$  below  $T_g$ .

Scherer used the fictive temperature to derive an analytic description of relaxation processes in the glassy state by extending the Adams–Gibbs–DiMarzio theory considering the fictive temperature for the calculation of the configurational entropy [26]. This Adam–Gibbs–Scherer (AGS) model results in the

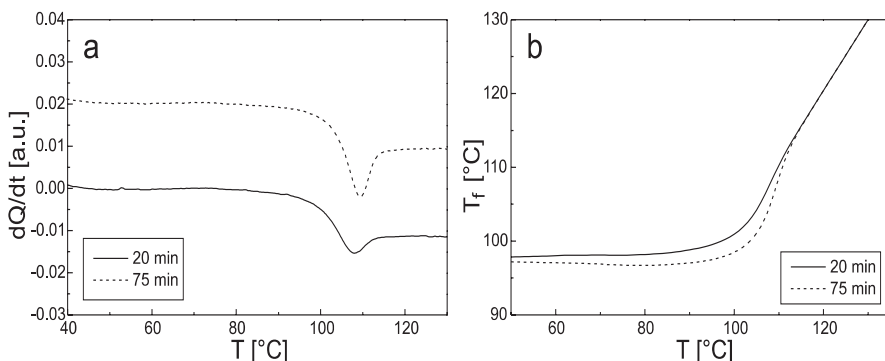


**Fig. 12.11.** (a) DSC curves (shifted by an offset for better visualization) and (b) calculated temperature dependence of the fictive temperature of polymer **1** after annealing at different temperatures

following expression for the time-temperature dependence of the relaxation process (in terms of the WLF notation) [15, 27]:

$$\ln \left[ \frac{\tau_m(T, T_f(T))}{\tau(T_g)} \right] = \frac{C_1 C_2}{T \left( 1 - \frac{T_g - C_2}{T_f(T)} \right)} - C_1. \quad (12.20)$$

For the case of a constant  $T_f$ , which is nearly the case according to DSC experiments (Fig. 12.11b), this equation predicts indeed the Arrhenius-type behavior of  $\tau_m(T)$  in the glassy state that was found in SHG and acoustoelectric measurements. The AGS model is also in accordance with relaxation behavior measured above and below the glass transition temperature as shown in Fig. 12.12. The temperature dependence of relaxation times observed on the side-chain NLO polymer **3** with dielectric spectroscopy above [20] and by SHG below the glass transition are well described by the AGS model (solid line).

In conclusion, our experiments showed a similar relaxation behavior for second order nonlinear optical and piezoelectric properties, although they are determined by different polar order parameters, and confirmed the theoretical prediction in [28]. The observed Arrhenius type temperature dependence of the relaxation time constants (also reported e.g. in [19, 29]) can be explained by the AGS model, which was discussed in similar way in [27, 30]. One may conclude from this result that a NLO polymer is the better suitable for application in electrooptic devices the higher its glass transition temperature is. A high  $T_g$  implicates however such problems as a reduced poling efficiency (because of the Boltzmann factor) and the chemical instability of NLO chromophores at high temperatures. Alternative approaches to stabilize the polar order have been discussed: Cross linking of the NLO polymers during poling [31, 32] may improve the poling stability but on the cost of disadvantages

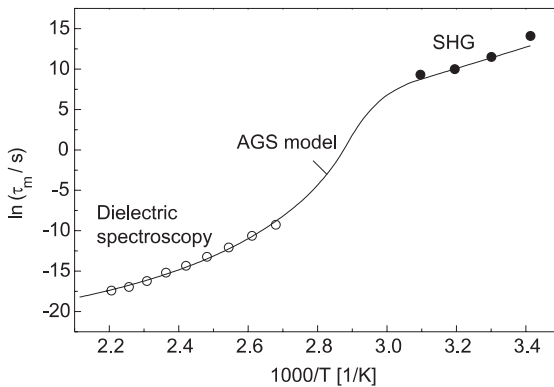


**Fig. 12.12.** Temperature dependence of relaxation time constants of the polymer **3** measured with dielectric spectroscopy and SHG above and below  $T_g$ , respectively, (dots) and a fit of the AGS model (solid line)

as a worse processability or a reduced polar order [33]. Enforcing the polar order by application of a permanent high d.c. voltage [34] is probably impracticable for real devices. Hence, the selection of the appropriate material for electrooptic devices is not only a question of the poling stability but a trade-off between several important material properties and some decrease of the electrooptic coefficient may be acceptable and compensated by an increase of the driving voltage.

## 12.4 Electroabsorption spectroscopy as a tool for relaxation measurements

### 12.4.1 Experimental technique

The detected signals in an electro-absorption spectrometer are the static component  $I$  and the electric field induced change  $\Delta I$  of the transmitted light intensity (Fig. 12.13). Since  $\Delta I \ll I$  the absorption change can be approximated by  $\Delta A = -\Delta I/I \ln 10$ . It makes the measurement insensitive to any specific spectral dependencies of the detector and allows for a comparable simple experimental set-up without sophisticated spectral calibration. A comparison of spectra obtained with and without a d.c. electric field applied does usually not suffice to determine the Stark effect because  $\Delta A$  is small and might not exceed the noise level. The signal-to-noise ratio can be improved by several orders of magnitude using an a.c. electric field and a lock-in amplifier. If an electric field  $E(t) = E_0 \sin(\Omega t)$  with a modulation frequency  $f = \Omega/2\pi$  is applied to the sample, the linear effect will also be observed at  $f$ . The quadratic effect is proportional to  $E^2(t)$  and has, because of  $E_0^2 \sin^2(\Omega t) = 0.5 E_0^2 [1 - \cos(2\Omega t)]$ , a d.c. component and a component at  $2f = \Omega/\pi$ . Since a lock-in amplifier typically delivers effective values in both the  $f$  and the  $2f$  measurement mode, it is convenient to express the magnitude of all a.c. signals as effective values. We have thus for the linear effect

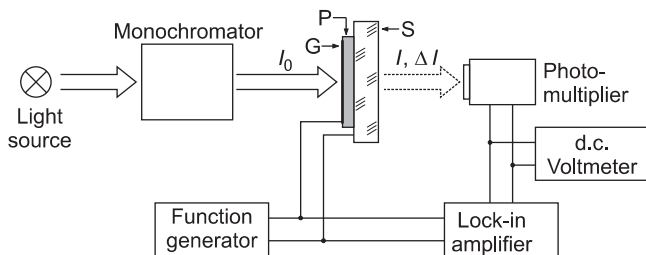


**Fig. 12.13.** Schematics of an electroabsorption spectroscopy experiment (G = semi-transparent gold electrode, P = polymer film, S = glass substrate with transparent ITO electrode),  $I_0$  incoming light intensity;  $I$ ,  $\Delta I$  see text



$$\Delta A_{\text{eff}}(f) = F_1 \frac{\Delta\mu E_{\text{eff}}(f)}{hc} \mathcal{A}'(\tilde{\nu}), \quad (12.21)$$

and for the quadratic effect

$$\Delta A_{\text{eff}}(2f) = \frac{E_{\text{eff}}^2}{\sqrt{2}} \left[ \frac{\Delta\alpha}{2hc} \mathcal{A}'(\tilde{\nu}) + \frac{(\Delta\mu)^2}{10h^2c^2} \mathcal{A}''(\tilde{\nu}) \right]. \quad (12.22)$$

Using measured absorption spectra  $A(\tilde{\nu})$  one can calculate the derivative terms  $\mathcal{A}'(\tilde{\nu})$  and  $\mathcal{A}''(\tilde{\nu})$  numerically. Fitting an equation of the form  $\Delta A(\tilde{\nu}) = C_1 \mathcal{A}'(\tilde{\nu}) + C_2 \mathcal{A}''(\tilde{\nu})$  with variable parameters  $C_1$  and  $C_2$  to an experimental quadratic electroabsorption spectrum  $\Delta A_{\text{eff}}^{2\omega}(\tilde{\nu})$  allows to determine the molecular parameters  $\Delta\mu$  and  $\Delta\alpha$ . The knowledge of the value of  $\Delta\mu$  allows then for the determination of the polar order parameter  $F_1$  after fitting an equation of the form  $\Delta A(\tilde{\nu}) = C_L \mathcal{A}'(\tilde{\nu})$  to the measured linear electroabsorption spectrum  $\Delta A_{\text{eff}}^{\omega}(\tilde{\nu})$  of a polar sample. Note that the polar order parameter can be calculated from

$$F_1 = \frac{C_L U_{\text{eff}}^{\text{qu}}}{\sqrt{10\sqrt{2}C_2 U_{\text{eff}}^{\text{lin}}}}, \quad (12.23)$$

where  $U_{\text{eff}}^{\text{qu}}$  and  $U_{\text{eff}}^{\text{lin}}$  are the modulation voltages used in the quadratic and linear experiment, respectively.  $F_1$  can therefore be determined without measuring the film thickness and without any assumption about the correction factors for the local field; esp. the latter reduces the error for the polar order parameter significantly and is a valuable advantage in comparison with other NLO measurements [35].

#### 12.4.2 Electroabsorption spectroscopy with variable modulation frequency

It has been desirable to study relaxation processes of NLO chromophores in polymers above and below the glass transition temperature, i.e. over several orders of magnitude in timescale, observing only one single physical property. New experimental techniques, often referred to as chi-electric relaxation measurements, have thus been developed for the observation of fast dynamics above the glass transition using quadratic NLO properties as e.g. SHG. The polar orientation of the chromophores is induced by a time dependent electric field  $E_p$  applied to the sample. The variation of the temporal relation between probing laser pulses and poling field allows to measure the temporal response of the NLO chromophore to the electric field. Figure 12.14 depicts the principles of two of the methods for chi-electric relaxation measurements. In Fig. 12.14a measurements are performed in the time domain [30]:  $E_p$  is a pulse of duration  $t_d$  and induces a second-order nonlinear susceptibility  $\chi^{(2)}$  that follows the electric field with a characteristic response time. The variation of the delay  $t_m$  between probing laser pulse  $I_\omega$  and  $E_p$  allows to determine

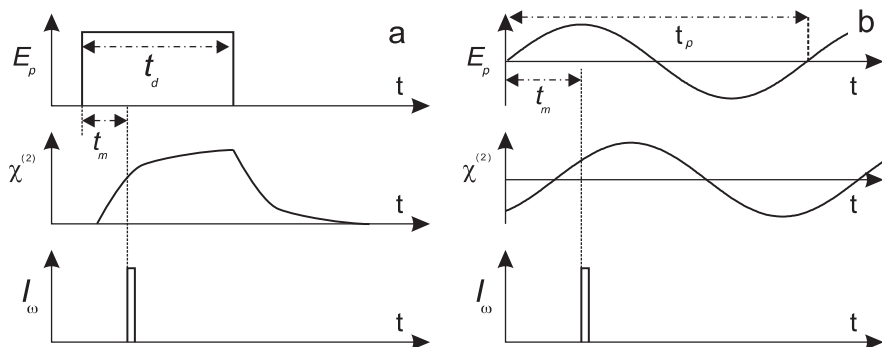


**Fig. 12.14.** Methods for chi-electric relaxation measurements in (a) time domain and (b) frequency domain (*top*: applied electric field, *middle*: response of nonlinear susceptibility  $\chi^2$ , *bottom*: probing laser pulse intensity)

the response characteristics of the field induced  $\chi^{(2)}$ . As shown in Fig. 12.14b a sinusoidal  $E_p$  (with oscillation time  $t_p$ ) induces a  $\chi^{(2)}$  response that is also sinusoidal and, in general, phase shifted [36]. Variation of the delay time  $t_m$  for the synchronization of the probing laser pulses with  $E_p$  allows to scan the SHG response and thus to determine the amplitude and phase shift of  $\chi^{(2)}$  (with respect to  $E_p$ ). Repeating the measurements at a number of different frequencies  $f = 1/t_p$  in the interesting frequency range allows to characterize the response characteristics of the NLO chromophores in the frequency domain. The measured SHG signal in both methods is however in fact the sum of  $\chi^{(2)}$  and  $\chi^{(3)}$  effects, where one of the field components in the  $\chi^{(3)}$  term of (12.1) is from the electric field  $E_p$ , whereas the other two components are from the electric field of the laser pulse. This  $\chi^{(3)}$  contribution to the apparent effect doesn't require reorientation of the chromophores, is much faster due to its electronic nature and appears thus as a constant offset.

The method for the measurement of the  $\chi^{(2)}$  response is not limited to SHG; the electrooptic (Pockels) effect or the electroabsorption (Stark) effect may be used as well. Both effects are the optical response (in dispersion and absorption, respectively) to an electric field. Measurements in the frequency domain may thus be performed using a sinusoidal electric field for both, inducing the polar order and measuring the electrooptic or electroabsorption response. Our research in this direction has been focused on the Stark effect after we observed the influence of an electric field on the electroabsorption signal due to reorientation of chromophores [37].

Electroabsorption spectroscopy as described above allows in general to distinguish between the  $\chi^{(2)}$  and the  $\chi^{(3)}$  contributions, which correspond to the linear and quadratic Stark effect, respectively, due to their different wavenumber dependency. As described in (12.12) and (12.21) the linear electroabsorption effect can be observed at the first harmonic  $f = \Omega/2\pi$  of the modulation field  $E(t) = E \exp(i\Omega t)$  and is proportional to the polar order

parameter  $F_1$ , whereas the quadratic effect is observable at the second harmonic  $2f$  and is (in good approximation) independent of  $F_1$ . The linear effect doesn't contribute to the signal at  $2f$  if the orientation of the chromophores is fixed. In the case of a sufficient rotational mobility at the frequency  $f$  a time dependent dipolar order may be induced by the modulation field  $E_m$ . In this case the polar order parameter  $F_1$  oscillates with the frequency  $f$ , i.e.

$$F_1(t) = M_1 E \exp(i\Omega t) = \sqrt{2} M_1 E_{\text{eff}} \exp(i\Omega t), \quad (12.24)$$

where  $M_1$  describes the magnitude of the chromophores' reorientation in the electric modulation field  $E_m(f)$  at the frequency  $f$ .

Another contribution to the apparent electroabsorption spectrum is based on the absorbance change through the reorientation itself. The electric field gives a slight preference for molecules oriented in the direction of the light propagation ( $z$  axis) and thus reduces the absorbance of the sample, which is proportional to the expectation value  $\langle \sin^2 \theta \rangle$  for the angle between the molecular long axis and the  $z$  axis. The effect is (in contrast to the linear and quadratic Stark effect) proportional to the absorption spectrum  $A(\tilde{\nu})$  itself and is quadratic in the electric modulation field  $E_m$ . Both, the oscillating polar order and the electro-orientation introduce additional contributions to the electroabsorption response at  $2f$ . Thus the electroabsorption spectrum can be described by

$$\Delta A_{\text{eff}}(2f) = \frac{E_{\text{eff}}^2}{\sqrt{2}} \left[ \frac{2M_1 \Delta\mu + \Delta\alpha}{2hc} \mathcal{A}'(\tilde{\nu}) + \frac{(\Delta\mu)^2}{10h^2 c^2} \mathcal{A}''(\tilde{\nu}) + M_0 A(\tilde{\nu}) \right]. \quad (12.25)$$

Taking into account the maximum values for both coefficients  $M_1$  and  $M_0$  according to the Boltzmann distribution of dipoles  $\mu_g$  in the electric field  $E$ , we can write

$$M_1 = \frac{1}{5} \eta \frac{\mu_g}{k_B T} \quad \text{and} \quad M_0 = \frac{1}{15} \eta \left( \frac{\mu_g}{k_B T} \right)^2, \quad (12.26)$$

where  $\eta$  is the relative response function that describes the reorientation magnitude in respect to its maximum ( $\eta = 0$  for orientational fixed chromophores,  $\eta = 1$  for chromophores that fully follow the modulation field  $E$ ).

Figure 12.15a shows the electroabsorption spectra of Disperse Red 1 (DR1, Fig. 12.1) in polymethylmethacrylate (PMMA) measured with modulation frequencies  $f = 2$  Hz and 2 kHz [38]. At  $f = 2$  kHz the chromophores are not able to follow the modulation field, whereas for  $f = 2$  Hz the reorientation of the chromophores is possible; the signal has thus a different amplitude and wavenumber dependency. The reorientation magnitude  $\eta$  can be evaluated by analyzing the relative magnitude of the different spectral contributions ( $A$ ,  $\mathcal{A}'$ ,  $\mathcal{A}''$ ) to the experimental electroabsorption spectra  $\Delta A(\tilde{\nu})$ . After fitting an equation of the form  $\Delta A(\tilde{\nu}) = C_0 A(\tilde{\nu}) + C_1 \mathcal{A}'(\tilde{\nu}) + C_2 \mathcal{A}''(\tilde{\nu})$  to experimental data,  $\eta$  is obtained by comparing the fit parameters  $C_0$  and  $C_1$  with the

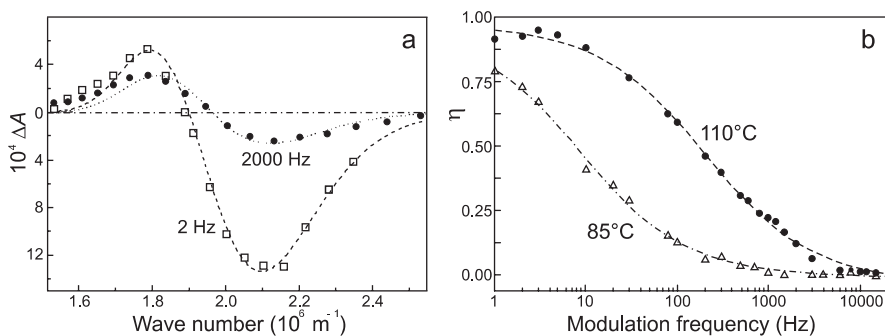


**Fig. 12.15.** Electroabsorption spectroscopy with variable modulation frequency. (a) Spectrum for Disperse Red 1 in PMMA for  $f = 2$  Hz and 2 kHz. (b) Frequency dependence of the reorientation magnitude  $\eta$  for two temperatures

expressions of the corresponding coefficients given in (12.25). In experiments we found  $C_0$  more significant than  $C_1$  because of the magnitude of this contribution and its direct proportionality to  $\eta$ . To determine the mean relaxation frequency and the relaxation frequency distribution one has to repeat the measurement of the electroabsorption spectra several times at different modulation frequencies  $f$  and calculate the corresponding  $\eta$  value. Figure 12.15b shows as an example the results obtained for DR1 in PMMA at two different temperatures. More detailed analyses have shown that the curves  $\eta(f)$  can be described by well-known frequency-domain relaxation functions (the dashed curves in Fig. 12.15b were obtained by fitting the Cole–Cole model). The corresponding mean relaxation frequencies are in agreement with results obtained by other techniques as chi-electric measurements [39–41].

Hence, electroabsorption spectroscopy with variable modulation frequency proved to be an alternative to other methods for the measurement of molecular orientation relaxation. The non-ambiguous attribution of the measured effect to the chromophore relaxation is a very important advantage over bulk measurements as dielectric spectroscopy and might be interesting for investigations on other materials besides quadratic NLO polymers, e.g. low- $T_g$  photorefractive polymers. Electroabsorption measurements are also possible on samples with very low chromophore concentration, which may be important to exclude or even study effects of aggregation. A certain disadvantage of this method is the requirement to measure full spectra  $\Delta A(\tilde{\nu})$  for a number of different modulation frequencies. However, in many cases it might be sufficient to determine the modulation frequency dependence of electroabsorption at a fixed wave number  $\tilde{\nu}$ . E.g. in Fig. 12.15a the response at  $\tilde{\nu} = 2.1 \times 10^6 \text{ m}^{-1}$  would be a good choice, because the signal magnitude is (besides a small frequency-independent offset) almost proportional to  $\eta$ .

### 12.4.3 Internal electric field in NLO films

In Sect. 12.3 we discussed briefly the influence of charges on the SHG or acoustoelectric signals. However, little attention (with some exceptions, see e.g. [42]) has been paid to understand effects related to charge transport and storage as well as non-uniform electric field distributions in NLO polymers, although these phenomena are relevant for both, preparation and operation of NLO polymer devices. From special importance is the knowledge of the internal electric field distribution from an externally applied voltage for poling [43, 44] or adjustment of retardation in modulators in Mach–Zehnder interferometer configuration [45]. Waveguide modulators consist usually of three different polymer layers, where the active layer (the NLO polymer) is embedded between two NLO inactive cladding layers. Since there is no method to measure the field distribution directly, one has to estimate it from its effect on other phenomena. To determine the electric field  $E_0$  within the active layer one may measure NLO properties but their field dependence may be unclear because a mixture of  $\chi^{(2)}$  and  $\chi^{(3)}$  effects is observed. An effect that is directly proportional to the field in the NLO active layer is thus very helpful for the investigation and understanding of the processes in polymeric sandwich structures under electric field. In the following we will show that electroabsorption is especially suitable for this task and present measurements that demonstrate the behavior of a nonuniform field distribution in a double-layer polymer film.

Above we discussed electroabsorption spectroscopy in terms of the linear Stark effect (observed at the frequency  $f$ ) of the modulation field  $E_f$  and the quadratic Stark effect, which can be measured at  $2f$ . In the presence of a d.c. electric field  $E_0$  (from an externally applied d.c. voltage or as result of internal polarization) the quadratic effect will however also contribute to the signal at  $f$ . It will be referred to as *quasilinear Stark effect* and is described by

$$\Delta A_{\text{eff}}^{\text{ql}}(f) = 2E_{\text{eff}}^2 E_0 \left[ \frac{\Delta\alpha}{2hc} \mathcal{A}'(\tilde{\nu}) + \frac{(\Delta\mu)^2}{10h^2c^2} \mathcal{A}''(\tilde{\nu}) \right], \quad (12.27)$$

i.e. it has the same wave number dependency as the quadratic effect (12.22). If the sample is polar the electroabsorption spectrum measured at  $f$  is the sum of the linear and the quasilinear effects. Figure 12.16 shows as an example the quasilinear and the linear electroabsorption spectrum of the NLO chromophore DMANA (Fig. 12.1) in polycarbonate [38]. Note two important points in the spectra: At wave number  $\tilde{\nu}_A$  the quasilinear effect is zero and only the linear effect contributes to the signal, whereas at  $\tilde{\nu}_B$  only the quasilinear effect will be measured. Since the latter is proportional to the electric field strength  $E_0$ , one may determine the magnitude and the temporal evolution of the internal field  $E_0$  by measuring the Stark signal at  $\tilde{\nu}_B$  [46, 47].

To demonstrate the usefulness of the method we performed experiments on double-layer sandwich structures (one active and one inactive layer,

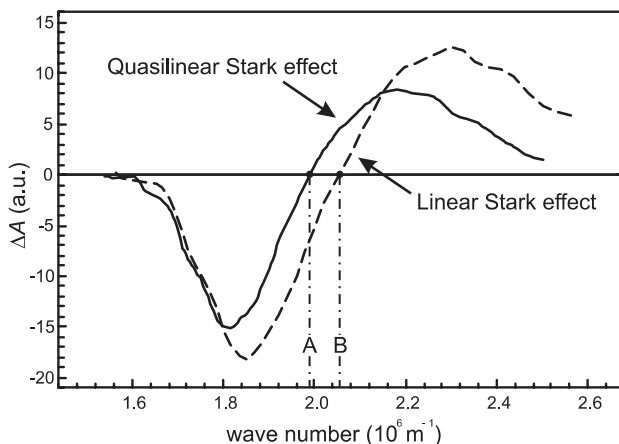


**Fig. 12.16.** Quasilinear and linear electroabsorption spectrum of the chromophore DMANA in polycarbonate.  $\tilde{\nu}_A$  corresponds to  $\lambda = 501$  nm,  $\tilde{\nu}_B$  to 488 nm

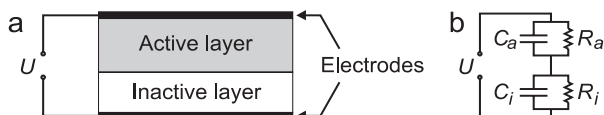


**Fig. 12.17.** Double polymer layer sandwich structure and simple equivalent circuit

Fig. 12.17a). The active layer consisted of  $4\ \mu\text{m}$  polycarbonate bisphenol-A containing 2 weight-% of the NLO chromophore DMANA, for the  $8.5\ \mu\text{m}$  thick inactive layer the polyimide PI 2566 was used. Figure 12.18 shows the evolution of the electroabsorption response measured with the modulation frequency  $f$  at  $488\ \text{nm}$  ( $\hat{=} \tilde{\nu}_B$ ), where the linear effect is zero [38]. During the first 500 seconds no d.c. voltage was applied to the sample and the response is zero within error range. At  $t = 0$  s the d.c. voltage was switched on and we observed an immediate response followed by a slower increase of the signal magnitude. A fast signal jump (in opposite direction) was also observed when the d.c. voltage was switched off at  $t = 1000$  s. The signal returns however not to zero but relaxes slowly with approximately the same time constant of  $\tau \approx 430$  s as observed at the process between  $t = 0$  s and 1000 s.

The equivalent circuit shown in Fig. 12.17b is the simplest model to describe the observed behavior. It considers that the layers have in general different resistance and capacitance, depending on the conductivity, dielectric constant and thickness of the respective layer. Immediately after a d.c. voltage  $U$  is applied to the electrodes of the sandwich structure at  $t = 0$  the voltage  $U_a^0$  across the active layer is determined by the capacitances of the layers, i.e.  $U_a^0 = UC_a/(C_a + C_i)$ . Then the conductivity of the layers allow charges to accumulate at the interface between active and cladding layer until the voltage  $U_a^\infty$  across the active layer for  $t \rightarrow \infty$  is determined

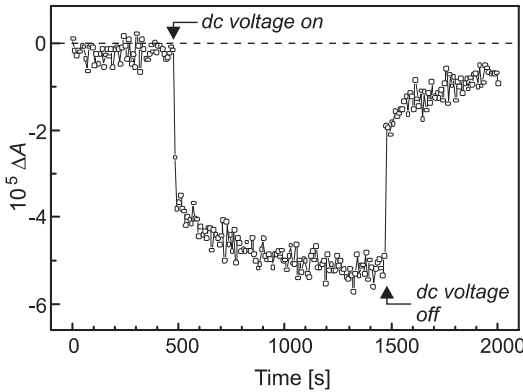


**Fig. 12.18.** Quasilinear Stark effect measured on a two-layer polymer sample

by the resistances, i.e.  $U_a^\infty = UR_a/(R_a + R_i)$ . According to the equivalent circuit the transition between  $U_a^0$  and  $U_a^\infty$  follows an exponential behavior  $U_a(t) = U_a^\infty - (U_a^0 - U_a^\infty) \exp(-t/\tau)$  with  $\tau = (C_a + C_i)/(R_a^{-1} + R_i^{-1})$ . Considering the dielectric constants of the polymers, thickness of the layers, the measured capacitance and resistance of the sample we find that the measured time constant ( $\tau \approx 430$  s) is in accordance with the two-layer equivalent circuit.

Comparable measurements on single-layer films reveal that an internal electric field may also be induced by charging effects on the polymer-electrode interface [47]. Such effects are important for the understanding of the properties of other sandwich structures, esp. organic light emitting diodes and solar cells. Electroabsorption spectroscopy has recently been used to determine the internal electric field in both structures [48, 49].

## 12.5 Summary

We presented investigations on relaxation phenomena in nonlinear optical polymers with focus on the stability of polar order after poling and the application of electroabsorption spectroscopy for relaxation measurements. The decay of the second order nonlinear optical susceptibility  $\chi^{(2)}$  in the glassy state of the polymers was measured by SHG and compared with piezoelectric measurements. The relaxation behavior for both cases was similar and could be described by an Arrhenius-type temperature dependence of the mean relaxation time. This result can be understood in frames of Scherer's extension of the Adams–Gibbs–DiMarzio theory for the glassy state.

We demonstrated that the electroabsorption spectra of NLO chromophores in polymers depend on the modulation frequency  $f$  used in the electroabsorption spectrometer if  $f$  is in the range of the chromophores' orientational relaxation frequency. The relaxation time constant can thus be obtained by

analyzing the spectra for a number of different suitable  $f$  values. This method allows one to measure chromophore relaxation above or in the glass transition region optically (i.e. in absorption) and is hence only sensitive to the absorbing chromophores. It can be considered as a valuable supplement to other techniques (e.g. dielectric spectroscopy) and can be compared with chi-electric relaxation measurements.

We also showed that anisotropic field distributions – especially in multi-layer polymer films – and their evolution can be studied by the Stark effect. For the appropriate wavelength the Stark effect is directly proportional to the internal electric field in the polymer layer that contains the NLO chromophores. It can thus be used to determine the response of the internal field to changes of the externally applied voltage. This is of specific importance for optimized poling, in polymeric light-emitting diodes and solar cells, where polarization effects at layer interfaces strongly influence the device performance.

**Acknowledgment.** Several co-workers of the authors contributed due to their experimental work: S. Großmann investigated double-layer polymer films, E. Jakob performed dielectric spectroscopy measurements and S. Saal developed the variable-modulation-frequency electroabsorption spectroscopy experiments. Valuable discussions with S.V. Yablonskii and L.M. Blinov are gratefully acknowledged. Part of the work was supported by the Volkswagen-Stiftung.

## References

1. D. Chen, H.R. Fetterman, A. Chen, W.H. Steier, L.R. Dalton, W. Wang, Y. Shi: Appl. Phys. Lett. **70**, 3335 (1997)
2. Y. Shi, W. Lin, D.J. Olson, J.H. Bechtel, H. Zhang, W.H. Steier, C. Zhang: Science **288**, 119 (2000)
3. G.R. Meredith, J.G. VanDusen, D.J. Williams: Macromolecules **15**, 1385 (1982)
4. J. Zyss, J.L. Oudar: Phys. Rev. A **26**, 2028 (1982)
5. K.D. Singer, M.G. Kuzyk, J.E. Sohn: J. Opt. Soc. Am. B **4**, 968 (1987)
6. A.F. Garito, C.C. Teng, K.Y. Wong, O. Zammami'Khamiri: Mol. Cryst. Liq. Cryst. **106**, 219 (1984)
7. D.A. Kleinman: Phys. Rev. **126**, 1977 (1962)
8. K.D. Singer, J.E. Sohn, S.J. Lalama: Appl. Phys. Lett. **49**, 248 (1986)
9. K.D. Singer, A.F. Garito: J. Chem. Phys. **75**, 3572 (1981)
10. W.F. Brown: In: *Dielektrika, Handbuch der Physik*, Vol. XVII, ed. by S. Flügge (Springer, Berlin 1956), pp. 1–154
11. C. Poga, T.M. Brown, M.G. Kuzyk, C.W. Dirk: J. Opt. Soc. Am. B **12**, 531 (1995)
12. M.I. Barnik, L.M. Blinov, T. Weyrauch, S.P. Palto, A.A. Tevosov, W. Haase: 'Stark Spectroscopy as a Tool for the Characterization of Poled Polymers for Nonlinear Optics'. In: *Polymers for Second-Order Nonlinear Optics*, ACS Symposium Series, Vol. 601, ed. by G.A. Lindsay, K.D. Singer (American Chemical Society, Washington, DC 1995), pp. 288–303



13. M.G. Broadhurst, G.T. Davis: In *Electrets*, Topics in Applied Physics, Vol. 33, 2nd edition, ed. by G.M. Sessler (Springer, Berlin 1987), pp. 285–319
14. F.I. Mopsik, M.G. Broadhurst: *J. Appl. Phys.* **46**, 4204 (1975)
15. T. Weyrauch: ‘Untersuchungen zur Polung und Relaxation nichtlinearer optischer Polymere.’ PhD Thesis, Technische Hochschule Darmstadt, Darmstadt (1997)
16. P.D. Maker, R.W. Terhune, M. Nisenoff, C.M. Savage: *Phys. Rev. Lett.* **8**, 21 (1962)
17. S.V. Yablonskii, E.I. Kats, M.V. Kozlovskii, T. Weyrauch, E.A. Soto Bustamante, D.B. Subachius, W. Haase: *Mol. Mater.* **3**, 311 (1994)
18. C.P.J.M. van der Vorst, R.A.P. van Gassel: *Macromol. Symp.* **90**, 47 (1995)
19. A. Dhinojwala, G.K. Wong, J.M. Torkelson: *Macromolecules* **26**, 5943 (1993)
20. E. Jakob, T. Weyrauch, T. Hanemann, W. Haase: ‘Relaxation Studies on a Polymethylmethacrylate with a Nitrostilbene Side Chain for Nonlinear Optics’. In: *Organic Materials for Nonlinear Optics III*, ed. by G.J. Ashwell, D. Bloor (Royal Society of Chemistry, Cambridge 1993), pp. 163–169
21. T. Weyrauch, R. Willner, E. Jakob, W. Haase: ‘Relaxation of Piezoelectricity and Nonlinear Optical Properties of Poled Polymers’. In: *Nonlinear Optical Properties of Organic Materials VI*, Proc. SPIE 2025, ed. by G.R. Möhlmann (SPIE, Bellingham, WA 1993), pp. 211–220
22. M.L. Williams, R.F. Landel, J.D. Ferry: *J. Amer. Chem. Soc.* **77**, 3701 (1955)
23. G. Adams, J.H. Gibbs: *J. Chem. Phys.* **43**, 139 (1965)
24. J.H. Gibbs, E.A. DiMarzio: *J. Chem. Phys.* **28**, 373 (1958)
25. A.Q. Tool: *J. Am. Ceram. Soc.* **29**, 240 (1946)
26. G.W. Scherer: *J. Am. Ceram. Soc.* **67**, 504 (1984)
27. H.-J. Winkelhahn, Th.K. Servay, D. Neher: *Ber. Bunsenges. Phys. Chem.* **100**, 123 (1996)
28. J.W. Wu: *J. Opt. Soc. Am. B* **8**, 142 (1991)
29. Ph. Prêtre, P.G. Kaatz, U. Meier, P. Günther, B. Zysset, M. Ahlheim, M. Stähelin, F. Lehr: *Polymer Preprints* **35**, 136 (1994)
30. R.D. Dureiko, D.E. Schuele, K.D. Singer: *J. Opt. Soc. Am. B* **15**, 338 (1998)
31. M. Eich, B. Reck, D.Y. Yoon, C.G. Willson, G.C. Bjorklund: *J. Appl. Phys.* **66**, 3241 (1989)
32. T. Hanemann, C. Noel, W. Haase: *Adv. Mater.* **7**, 465 (1995)
33. J.D. Bewsher, G.R. Mitchell: *Appl. Opt.* **36**, 7760 (1997)
34. A. Chen, V. Chuyanov, S. Garner, H. Zhang, W.H. Steier, J. Chen, J. Zhu, F. Wang, M. He, H. Mao, L.R. Dalton: *Opt. Lett.* **23**, 478 (1998)
35. S. Großmann, T. Weyrauch, W. Haase: *J. Opt. Soc. Am. B* **15**, 414 (1998)
36. W.N. Herman, J.A. Cline: *J. Opt. Soc. Am. B* **15**, 351 (1998)
37. L.M. Blinov, S.P. Palto, A.A. Tevosov, M.I. Barnik, T. Weyrauch, W. Haase: *Mol. Mater.* **5**, 311 (1995)
38. S. Großmann, T. Weyrauch, S. Saal, W. Haase: ‘Characterization of NLO Materials for Photonic Application’. In *Anisotropic Organic Materials – Approaches to Polar Order*, ACS Symposium Series, Volume 798, ed. by R. Glaser and P. Kaszynski (American Chemical Society, Washington, DC 2001) pp. 2–15
39. W. Haase, S. Saal, S. Großmann, T. Weyrauch: ‘Mobility of Dyes in Polymer Matrix: Frequency-dependent Electroabsorption’. In: *Organic Photonic Materials and Devices*, Proc. SPIE 3623, ed. by B. Kippelen (SPIE, Bellingham, WA 1999), pp. 159–166

40. S. Saal, W. Haase: Chem. Phys. Lett. **278**, 127 (1997)
41. S. Saal: 'Elektroabsorptionsspektroskopie zur Charakterisierung der Rotationsmobilität von Farbstoffmolekülen in polymeren Matrices'. PhD Thesis, Technische Universität Darmstadt, Darmstadt (1999)
42. R. Blum, M. Sprave, J. Sablotny, M. Eich: J. Opt. Soc. Am. B **15**, 318 (1998)
43. D.G. Girton, W.W. Anderson, J.A. Marley, T.E. Van Eck, S. Ermer: In *Organic Thin Films for Photonics Applications*, OSA Technical Digest Series, Vol. 21, (Optical Society of America, Washington DC 1995), pp. 470–473
44. V. Ricci, G.I. Stegeman, K.P. Chan: J. Opt. Soc. Am. B **17**, 1349 (2000)
45. H. Park, W.-Y. Hwang, J.-J. Kim, Appl. Phys. Lett. **70**, 2796, (1997)
46. S. Großmann, T. Weyrauch, S. Saal, W. Haase: Opt. Mat. **9**, 236 (1998)
47. S. Großmann, T. Weyrauch, W. Haase: Nonlinear Optics **20**, 223 (1999)
48. T.M. Brown, J.S. Kim, R.H. Friend, F. Cacialli, R. Daik, W.J. Feast: Synthetic Metals **111–112**, 285 (2000)
49. P.A. Lane, J. Rostalski, C. Giebeler, S.J. Martin, D.D.C. Bradley, D. Meissner: Solar Energy Materials & Solar Cells **63**, 3 (2000)

Relaxation Phenomena

Liquid Crystals, Magnetic Systems, Polymers, High-Tc  
Superconductors, Metallic Glasses

Haase, W.; Wróbel, S. (Eds.)

2003, XXX, 716 p., Hardcover

ISBN: 978-3-540-44269-1